COMPARISON OF IN-SITU BALLOON-BORNE AND LIDAR MEASUREMENT OF CIRRUS CLOUDS

Thomas Kuhn[1], **Veronika Wolf**[1], **Peter Völger**[2], **Marin Stanev**[3], **and Jörg Gumbel**[3]

[1]*Luleå University of Technology, Department of Computer Science, Electrical and Space Engineering, Division of Space Technology, 98128 Kiruna, Sweden*
[2]*The Swedish Institute of Space Physics (IRF), Polar Atmospheric Research Programme, Kiruna, Sweden*
[3]*Stockholm University, Department of Meteorology (MISU), Stockholm, Sweden*

ABSTRACT

A series of in-situ balloon-borne experiments conducted at Kiruna, Sweden (68 °N), is studying upper-tropospheric, cold ice clouds in arctic latitudes. Experiments are launched from Esrange Space Center and collect ice particles with an in-situ imaging instrument. One of the aims with these measurements is to improve satellite remote sensing of cold ice clouds. Such clouds can be observed by lidar. Therefore, when possible, concurrent ground-based lidar measurements have been carried out with two available lidar systems to accompany the balloon-borne measurements. The Esrange lidar is located at Esrange Space Center, approximately 500 m from the in-situ launch site on the balloon pad; the IRF lidar is located about 29 km to the west of Esrange Space Center (operated by the Swedish Institute of Space Physics, IRF). Here we present results from these lidar measurements and compare them to ice particle properties determined during the in-situ measurements.

Key words: Cirrus; ice clouds; lidar; ice particles; in-situ; balloon-borne; Arctic; high latitude measurements.

1. INTRODUCTION

Upper-tropospheric cold ice clouds (cirrus) play an important role in the radiative energy budget of the atmosphere [1]. They can both have a cooling as well as a warming effect as they reflect part of the incoming shortwave radiation and absorb part of Earth's outgoing longwave radiation, respectively. The net effect depends on the various cloud's macro- and microphysical properties, such as size and shape of ice particles.

Cirrus can be detected remotely by lidar and cloud radar. However, they are often thin and are consequently better observed by the more sensitive lidar while they are invisible or very weak to the cloud radar [2]. For these cases improved satellite retrieval methods will allow better ice cloud determination by space-borne lidar only. Retrieval methods for remote sensing of ice cloud properties require good knowledge of the microphysical properties of ice clouds, as for example shapes and size distributions of ice particles [1, 3]. Also radiative transfer simulations and climate models that include cloud processes need such knowledge. In-situ measurements are therefore necessary to acquire these properties.

Many in-situ measurements have already been performed by aircraft-mounted instruments. A review of some of the recent campaigns can be found for example in [4]. However, there are some problems associated with aircraft-based instruments. Shattering of larger ice particles at the inlet due to high impact speed causes many smaller fragments that may be detected erroneously as many small ice particles [5]. Instruments can now correct for this and/or avoid shattering [6], but the problem can not be eliminated entirely [7]. Also, most in-situ aircraft instruments have problems detecting and sizing ice particles smaller than about 100 µm [8] and in addition shapes of these particles remain uncertain [9]. Balloon-borne measurements do not suffer from shattering problems and smaller ice particles can be measured more accurately [10, 11]. In addition, they directly measure near to vertical profiles, which is an advantage when comparing to vertically sensing lidar measurements and for radiative transfer simulations.

Compared to mid- or tropical latitudes, only few in-situ measurements, both aircraft- and balloon-borne, exist at northerly, arctic latitudes [e.g. 12]. Furthermore, only few direct comparisons between ground-based lidar and in-situ measurements have been done [e.g 13]. Therefore, we have started balloon-borne in-situ measurements of high latitude, upper-tropospheric, cold ice clouds with concurrent ground-based lidar measurements. In the following, we describe first comparisons between these lidar and in-situ measurements of ice clouds.

2. EXPERIMENTAL METHODS

2.1. Balloon-borne in-situ measurements

2.1.1. Balloon campaign

The in-situ measurements used in this study are from an ongoing campaign of balloon-borne measurements of ice cloud particles, 'in-situ IWC' [14, 11]. A series of balloon launches has started in 2012. All balloons are launched from Esrange Space Center (67.9 °N 21.1 °E), about 30 km east of Kiruna located in northern Sweden, north of the Arctic circle. On the campaign days, balloon measurements have been carried out during morning up to around local noon. This allows for recovery by helicopter at daylight on the same day. The balloons on the campaign days considered here were launched from around 9:30 to 11:30 UTC (10:30 to 12:30 local time).

2.1.2. In-situ measurement method

The instrument carried by balloon is collecting individual ice particles on an oil-coated film. Particles are shortly after collection imaged with a high-resolution camera system that allows measurements of small ice particles. From the particle images size, area, and shape of particles with sizes down to about 20 µm can be determined. In addition to these single particle properties, ensembles are characterised by number and area concentrations and size distributions. Details of the instrument and the related image analysis methods have been described earlier [11].

The extinction coefficient $\alpha_{\text{in-situ}}$ of an ensemble of sampled ice particles in a cirrus can be determined from the image data by determining the cross-sectional area of this ensemble of particles. The sum of the individual ice particle areas is divided by the corresponding sampling volume, which yields the area concentration. The extinction cross section of an individual ice particle is given by twice its cross sectional area in the geometric scattering case that is applicable here where particle dimension is much larger than the wavelength of visible light. Hence, the local extinction coefficient is given by twice the area concentration of a representative ensemble of ice particles at that location. Then, from the extinction coefficients throughout a cirrus, along the vertical profile sampled by the balloon-borne in-situ measurements, the optical depth $\tau_{\text{in-situ}}$ can be determined by integrating over $\alpha_{\text{in-situ}}$ vertically through the cirrus cloud.

2.2. Ground-based lidar measurements

2.2.1. Lidar systems

During the campaign, when possible, the balloon-borne in-situ measurements have been accompanied by concurrent lidar measurements by at least one of the two ground-based lidars, the lidar at IRF or at Esrange Space Center. The IRF lidar is located about 1 km from the Space Campus in Kiruna, which is around 3 km east of Kiruna airport and 29 km west of Esrange Space Center. This lidar is operated by the Swedish Institute of Space Physics (IRF). It uses elastic backscattering at 532 nm wavelength to detect clouds in an altitude range of 4 km to 15 km under daylight conditions. Data from the IRF lidar has a vertical resolution of 30 m and an averaging time of 133 s. More details about the IRF lidar can be found in [15].

The Esrange lidar is located at the Esrange Space Center on a hill that is around 500 m away from the location on the balloon pad where the in-situ balloons are launched. This lidar is operated by Stockholm University. It is a Rayleigh/Mie/Raman backscatter lidar. The lidar data used in this study uses the backscatter signals from the elastic low- and medium sensitivity Rayleigh channels at 532 nm wavelength covering the atmosphere from about 4 km to 30 km altitude during daylight conditions. The backscattered light is filtered through density tuned fixed-spacer etalons for that purpose. The Esrange lidar has a vertical resolution of 150 m and a time resolution of approximately 5 min. More details about the Esrange lidar can be found in [16].

2.2.2. Cirrus analysis with lidar

The free tropospheric aerosol in the measurement region in this study has very low concentrations compared to lower latitude locations in the northern hemisphere [17]. Therefore, we assume here that the lidar backscatter is caused only by atmospheric molecular scattering and backscatter from cirrus ice particles. Below and above clouds we expect only atmospheric backscatter. Below a cloud this signal is not affected by the cloud. Hence, there the signal can be predicted from the atmospheric molecular density, which is known from the temperature profile acquired by radio sonde measurements that accompany all balloon-borne measurements.

The backscatter signal from above a cirrus cloud can also be predicted, however, the signal is now attenuated by the presence of the cirrus. This attenuation, i.e. the optical depth of the cirrus cloud layer, can be determined by independently fitting the atmospheric backscatter below and above the cloud layer. The resulting factor between these two fits is attributed to attenuation of the cirrus and equal to its transmission squared, T^2_{cirrus}, which can be converted to its optical depth τ_{lidar} by

$$\tau_{\text{lidar}} = -\ln T_{\text{cirrus}} \tag{1}$$

For this purpose, the cloud bottom and top is determined for each lidar profile. Then the expected atmospheric scattering is fitted to the signal below the cloud bottom and above the cloud top.

Different methods exist for considering the molecular background within the cirrus layer, so that the fitted signals below the bottom and above top of the cirrus can be joined to form a continuos atmospheric molecular backscattering component S_{bg} of the signal, the atmospheric background scattering. This background can then be compared to the total signal within the cirrus layer, i.e. the sum of both signal components due to cirrus (S_{cirrus}) and atmospheric background scattering (S_{bg}). The ratio between the total backscatter and the background scattering signals is called backscatter ratio, or BSR.

$$\mathrm{BSR} = \frac{S_{\mathrm{cirrus}} + S_{\mathrm{bg}}}{S_{\mathrm{bg}}} \tag{2}$$

The backscatter ratio can also be expressed in terms of the backscatter coefficients for cirrus ($\beta_{\mathrm{lidar}}^{\mathrm{cirrus}}$) and background scattering($\beta_{\mathrm{lidar}}^{\mathrm{bg}}$):

$$\mathrm{BSR} = \frac{\beta_{\mathrm{lidar}}^{\mathrm{cirrus}} + \beta_{\mathrm{lidar}}^{\mathrm{bg}}}{\beta_{\mathrm{lidar}}^{\mathrm{bg}}} \tag{3}$$

The backscatter coefficient $\beta_{\mathrm{lidar}}^{\mathrm{bg}}$ of the background atmosphere can be determined from the atmospheric molecular density and the cross section of air molecules for backscattering at 532 nm (differential Rayleigh cross section of 6.1810^{-28} cm^2 sr^{-1}). From this, together with BSR, the cirrus' backscatter coefficient $\beta_{\mathrm{lidar}}^{\mathrm{cirrus}}$ can be inferred using Eq. 3. While no assumptions were required to determine the cirrus optical depth directly from comparisons of signals above and below the cirrus layer, now assumptions are needed to determine BSR and $\beta_{\mathrm{lidar}}^{\mathrm{cirrus}}$. Within the cirrus $\beta_{\mathrm{lidar}}^{\mathrm{bg}}$ needs to be known, hence, an assumption on how exactly $\beta_{\mathrm{lidar}}^{\mathrm{bg}}$ varies in the cirrus layer is required.

Even more assumptions are required to determine the extinction coefficient of the cirrus cloud, which is therefore the most uncertain cirrus optical property to be retrieved. This is due to the fact that there are two unknowns, the backscatter and extinction coefficients, and only one received backscatter signal [18, 19]. The ratio between cirrus extinction ($\alpha_{\mathrm{lidar}}^{\mathrm{cirrus}}$) and backscatter coefficients ($\beta_{\mathrm{lidar}}^{\mathrm{cirrus}}$) is called the lidar ratio L_{cirrus}. One needs to know L_{cirrus} so that $\beta_{\mathrm{lidar}}^{\mathrm{cirrus}}$ can be converted to $\alpha_{\mathrm{lidar}}^{\mathrm{cirrus}}$. Further, an assumption on how L_{cirrus} varies within the cirrus (and over time) is required. If we assume a constant L_{cirrus}, then

$$\alpha_{\mathrm{lidar}}^{\mathrm{cirrus}} = \beta_{\mathrm{lidar}}^{\mathrm{cirrus}} L_{\mathrm{cirrus}} \tag{4}$$

This can then be compared to the extinction coefficients $\alpha_{\text{in-situ}}$ determined from in-situ ice particle image data (see Sect. 2.1.2). Here, we assume a lidar ratio $L_{\mathrm{cirrus}} = 20$ sr, which is well within the large range of lidar ratios reported in the literature [e.g. 20, 21, 22].

3. MEASUREMENT RESULTS AND ANALYSIS

3.1. Measurement days

In-situ data have been collected on eight days so far from 2012-04-04 until 2016-12-15. Accompanying lidar data, however, are not available from all these days. On some occasions lidar measurements were not possible due to different reasons such as low-altitude liquid-phase clouds that were too optically thick obscuring the cirrus atop, ongoing lidar repairs/updates, or unavailability of lidar personnel. In the following Sections 3.2 and 3.3 lidar data from two days have been considered: 2013-02-20 (IRF and Esrange lidars) and 2016-02-12 (IRF lidar). On 2016-02-12 the cirrus originated from a warm front along the Swedish–Finish border associated to a strong low-pressure system over the northern Baltic Sea. On 2013-02-20 Kiruna was affected by a strong, northwesterly wind, which led to orographic lifting and mountain lee waves, causing a cirrus layer. The wind was originated from the cold front of a low-pressure system over Spitsbergen pushing air masses against a high-pressure system dominating Scandinavia.

3.2. 2016-02-12

3.2.1. Raw signals of IRF lidar

Fig. 1 shows the raw signal as a colour plot with all profiles measured by the IRF lidar on 2016-02-12. During the time of the balloon launch, from 9:40 to 10:40 UTC (10:40 to 11:40 local time), a cirrus layer can be seen between approximately 5 km and 8 km altitude. Altitude here refers to the lidar range, i.e. the vertical distance from lidar to the cloud layer from which backscattering is received. Later, when comparing lidar and in-situ data, the in-situ altitude (above sea level) is converted to range by subtracting 0.4 km, the actual altitude of the two lidars.

This cloud layer persisted for several hours, as long as measurements were recorded with the lidar. The figure shows at about 10:40 to 11:00 UTC (11:40 to 12:00 local time) an additional lower cloud layer at approximately 2 km altitude. It can be noted how this cloud layer is disturbing the cirrus observations above because it is attenuating the lidar signal.

As an example, Fig. 2 shows a backscatter signal with background noise removed of the IRF lidar on 2016-02-12 for one profile, at 9:38 UTC (10:38 local time). One can clearly see that the signal is predominantly caused by a cirrus layer between about 5 km and 10 km. The expected signal from atmospheric molecular backscattering (atmospheric background) is also shown for reference as dashed line. A second dashed line shows the same atmospheric background but scaled by a factor that can be attributed to attenuation by the cloud, i.e. its optical depth τ_{lidar} (see Sect. 2.2.2), which for this example was 2.0.

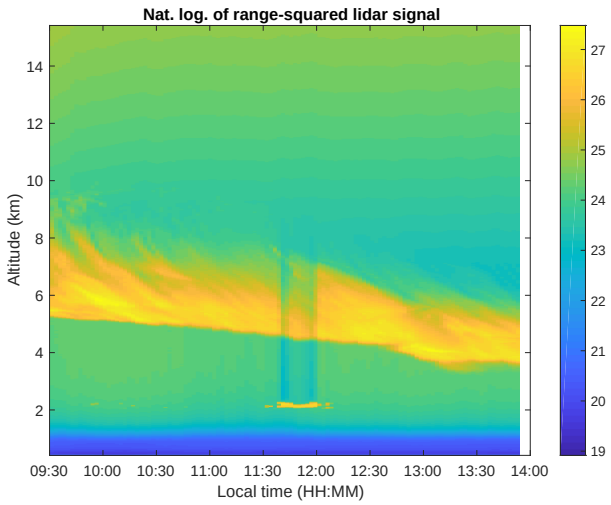

Figure 1. Raw signal of IRF lidar on 2016-02-12, range-squared.

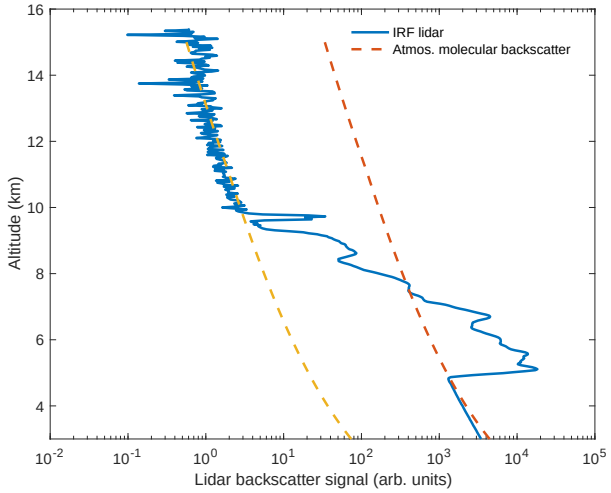

Figure 2. Backscatter signal of IRF lidar on 2016-02-12, at 9:38 UTC (10:38 local time). The atmospheric background is indicated as two dashed lines, one for the signal below and one for above the cirrus layer.

3.2.2. Collocation

The in-situ data on 2016-02-12 showed a cirrus layer between approximately 3.4 km and 7.7 km. That is a larger altitude range, and extending to lower altitudes compared to the lidar-measured cloud shown in Fig. 1. This is most likely caused by the fact that the lidar and the in-situ measurements do not happen at the same location. The IRF lidar is 29 km away from the Esrange balloon pad. Wind data from the radiosonde attached to the in-situ instrument showed that the wind from about 3 km altitude upwards came from S–SSW. At 5 km altitude it was from 209 ° at 9.1 m s^{-1}. This resulted in a closest horizontal distance between lidar observed air volume and in-situ measurement location of about 21 km at 5 km altitude. To reach this closest distance, the lidar observed air volume advected from the lidar 12 km in approximately 22 min, i.e the lidar measured at about 9:40 UTC a cloud that then advected closer to the location of in-situ measurement at the same altitude at about 10:00 UTC. Hence, lidar data from 9:40 UTC (10:40 local time) were chosen for comparison with in-situ data on that day. The balloon trajectory and the wind direction from the lidar are depicted in Fig. 3. Similarly, on 2013-02-20 an appropriate time for comparison was chosen to minimize the distance between lidar and in-situ measurements.

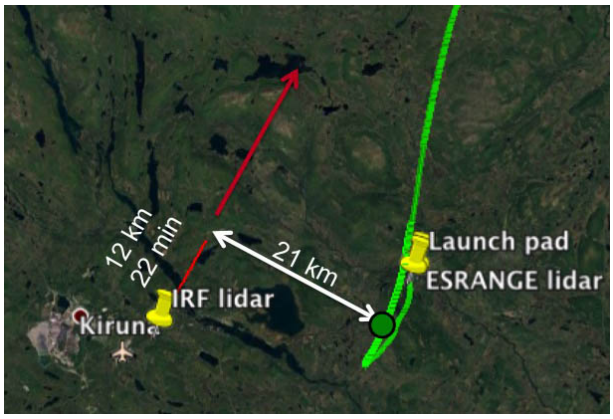

Figure 3. Balloon trajectory on 2016-02-12. The lidar location is marked as well as the wind direction at 5 km altitude, 209 °. Clouds observed at the lidar advect in this wind direction, along the red line in the figure. The location of the balloon at approximately 5 km altitude is indicated with a green circle. At this altitude it is about 21 km away (indicated with white arrow) from the line of clouds advecting from the lidar.

3.2.3. In-situ data

The cirrus cloud as measured with the in-situ instrument on 2016-02-12 extended from 3.40 km to 7.68 km altitude, with temperatures from −23 °C at the cloud bottom to −48 °C at the top. A total of 712 ice particles were analysed from this cloud. Fig. 4 shows the area size

distribution of these particles. It is determined from the number size distribution, which is multiplied, on a bin-by-bin basis, by the average area of the ice particles in the respective size bin. The total area concentration, the integral of the area distribution in Fig. 4, is 0.21 km^{-1} for 2016-02-12. Hence, the extinction coefficient, twice the area concentration (see Sect. 2.1.2), is 0.41 km^{-1}.

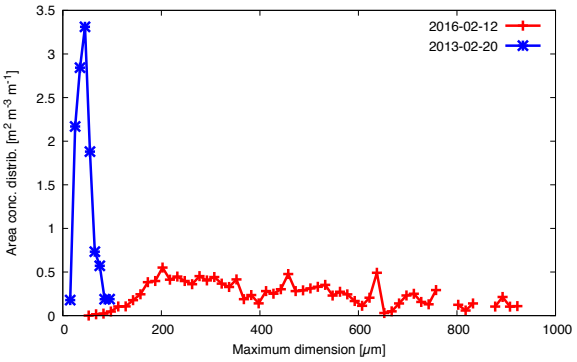

Figure 4. Area size distribution of cirrus clouds on 2016-02-12 and 2013-02-20.

When analysed in three layers, this cirrus had a lower extinction coefficient in the bottom layer, and a higher extinction in the top layer, compared to the value in the middle layer ($\alpha_{\text{in-situ}} = 0.094\,km^{-1}$ between 3.4 km and 4.5 km; 0.36 km^{-1} between 4.5 km and 5.6 km; and 0.81 km^{-1} between 5.6 km and 7.7 km). The number concentrations were 3.9 L^{-1} at the bottom, 13 L^{-1} in the middle, and 4.7 L^{-1} at the top.

The overall optical depth $\tau_{\text{in-situ}}$ of this cloud is 1.8, determined from vertically integrating the extinction coefficients or, equivalently, by multiplying the average extinction coefficient of 0.41 km^{-1} with the geometrical thickness of 4.3 km.

3.2.4. Extinction coefficient from lidar data

The extinction coefficients $\alpha_{\text{lidar}}^{\text{cirrus}}$, as described in Sect. 2.2.2, can be determined from BSR using Eq. 3 and Eq. 4. For an IRF lidar profile at about 9:40 UTC on 2016-02-12 the resulting extinction coefficient profile can be seen in Fig. 5.

Values for $\alpha_{\text{lidar}}^{\text{cirrus}}$ from lidar using BSR are generally smaller than values of $\alpha_{\text{in-situ}}$ from in-situ data (see Fig. 5). A possible explanation for this could be that the assumed lidar ratio L_{cirrus} was too small. However, the fact that lidar and in-situ instrument did not measure the cloud at the same location makes this reasoning uncertain.

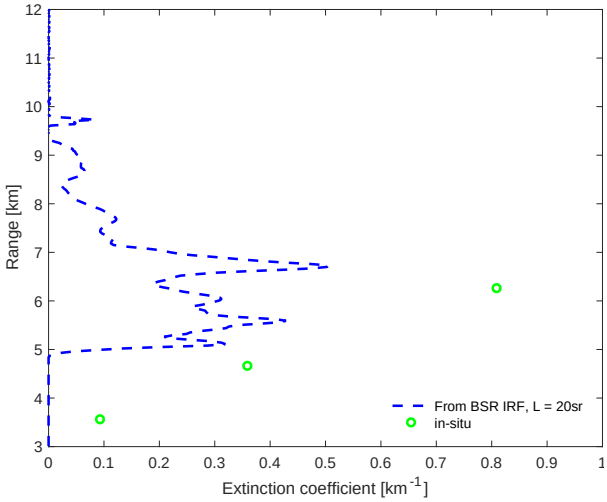

Figure 5. Extinction coefficient $\alpha_{\text{lidar}}^{\text{cirrus}}$ determined from BSR using Eq. 3 and Eq. 4 for 2016-02-12 at 9:38 UTC (10:38 local time) from the IRF lidar. For comparison, extinction coefficients $\alpha_{\text{in-situ}}$ are shown as well.

3.2.5. Optical depth

The optical depth τ_{lidar} is determined from the lidar attenuation, or transmission T_{cirrus} through the cloud as described in Sect. 2.2.2. No further assumptions have to be made for this. Alternatively, τ_{lidar} can be determined by integrating $\alpha_{\text{lidar}}^{\text{cirrus}}$ through the cloud. To first determine $\alpha_{\text{lidar}}^{\text{cirrus}}$, we had to assume the lidar ratio L_{cirrus}. Here we assumed a constant $L_{\text{cirrus}} = 20$ sr. If it was over- or underestimated, then also $\alpha_{\text{lidar}}^{\text{cirrus}}$ and with that τ_{lidar} will be over- or underestimated.

Fig. 6 shows time series of τ_{lidar} on 2016-02-12 determined using the two methods mentioned above. After about 10:30 UTC increased noise in the data due to the lower cloud observed in Fig. 1 caused problems determining τ_{lidar}. Before that, one can see that τ_{lidar} from integrating $\alpha_{\text{lidar}}^{\text{cirrus}}$ seems underestimated. This could be due to a too low assumption of L_{cirrus}, which would confirm our earlier reasoning when comparing $\alpha_{\text{lidar}}^{\text{cirrus}}$ with $\alpha_{\text{in-situ}}$ in Fig. 5.

3.3. 2013-02-20

3.3.1. In-situ data

On 2013-02-20 a cirrus was measured by the in-situ instrument between 9.0 km and 10.5 km altitude. Of all collected particles a representative sample of 279 has been analysed. These particles are from three layers within the continuous cloud: bottom, middle, and top. On this day, the particle concentrations were relatively high (86 L^{-1}, 220 L^{-1}, and 370 L^{-1} at the cloud bottom, middle, and top, respectively). Fig. 4 showed the area size distribution for the complete cirrus layer. The extinction coefficients

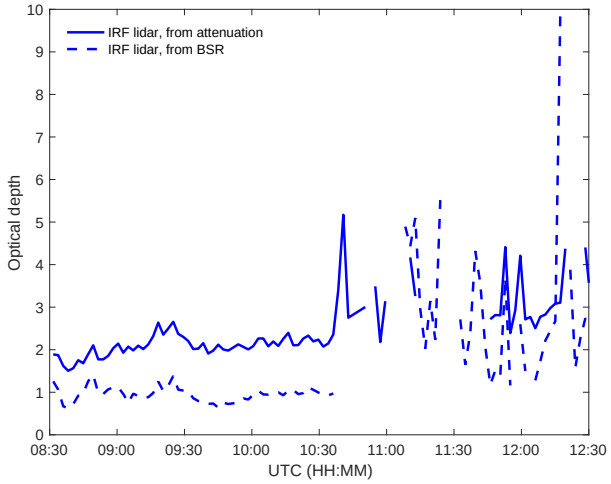

Figure 6. Optical depth τ determined from lidar measurements on 2016-02-12. Results from directly looking at attenuation of the signal from below to above the cloud and from integration of $\alpha_{\text{lidar}}^{\text{cirrus}}$, determined from BSR are compared.

in these three layers are $\alpha_{\text{in-situ}} = 0.22\,\text{km}^{-1}$ at around 9.2 km; $0.28\,\text{km}^{-1}$ at 9.8 km, and $0.26\,\text{km}^{-1}$ at 10.3 km. While number concentrations increased with increasing altitude and decreasing temperature (from $-56\,°\text{C}$ at the cloud bottom to $-66\,°\text{C}$ at the top), extinction coefficients stayed almost constant. The values for $\alpha_{\text{in-situ}}$, despite the higher number concentrations, were similar or lower than on 2016-02-12. The overall optical depth $\tau_{\text{in-situ}}$ on 2013-02-20 of 0.41, however, was smaller than on 2016-02-12 because of the cloud being geometrically thinner.

3.3.2. Extinction coefficient from lidar data

For lidar measurements on 2013-02-20, extinction coefficients $\alpha_{\text{lidar}}^{\text{cirrus}}$ determined from the BSR are shown in Figures 7, 8, and 9. On that day both lidars operated and profiles from about 11:00 UTC are shown in Fig. 9. After that time the IRF lidar was stopped due to increased stray light issues. The best time for comparison with the in-situ measurements would have been around 11:30 UTC. Profiles of $\alpha_{\text{lidar}}^{\text{cirrus}}$ from the Esrange lidar are shown for both these times.

On 2013-02-20 values for $\alpha_{\text{lidar}}^{\text{cirrus}}$ and $\alpha_{\text{in-situ}}$ were more similar than on 2016-02-12. However, the two profiles for the Esrange lidar show how much $\alpha_{\text{lidar}}^{\text{cirrus}}$ can vary in a short period of time of 30 min. Also in 4 min, from one profile to the next, $\alpha_{\text{lidar}}^{\text{cirrus}}$ may change by 50% in certain layers. The better agreement between $\alpha_{\text{lidar}}^{\text{cirrus}}$ and $\alpha_{\text{in-situ}}$ indicates that the assumed lidar ratio of 20 sr may be a better guess on this day.

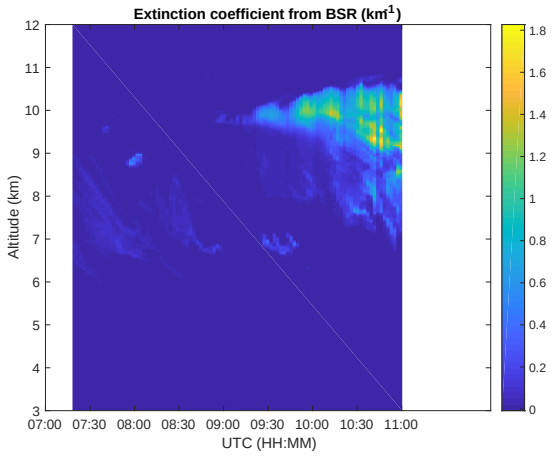

Figure 7. Extinction coefficients $\alpha_{\text{lidar}}^{\text{cirrus}}$ determined from BSR of IRF lidar on 2013-02-20.

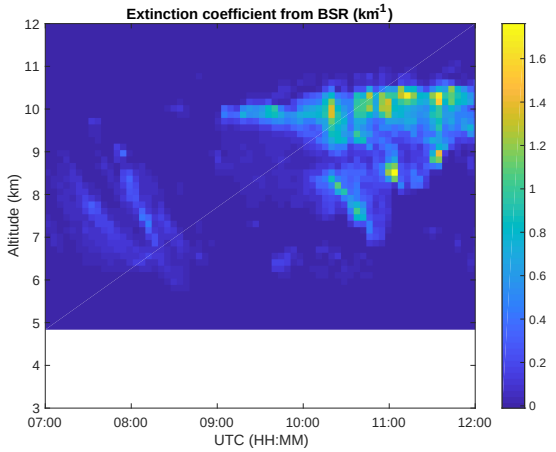

Figure 8. Extinction coefficients $\alpha_{\text{lidar}}^{\text{cirrus}}$ determined from BSR of Esrange lidar on 2013-02-20.

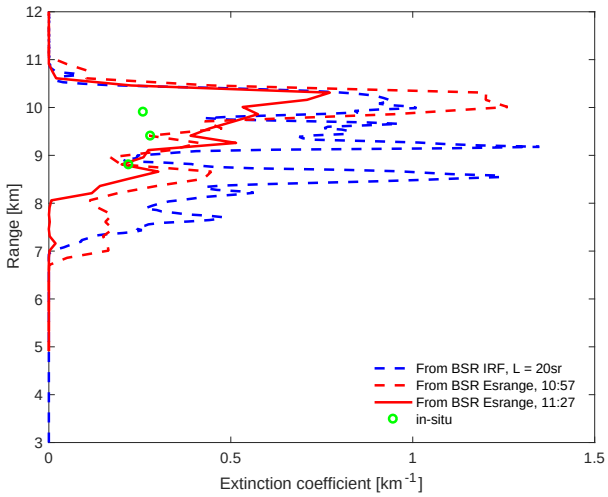

Figure 9. Extinction coefficient α_{cirrus} determined from BSR using Eq. 3 and Eq.4 for 2013-02-20 from the IRF and Esrange lidar, respectively.

3.3.3. Optical depth

Fig. 10 shows time series of τ_{lidar} on 2013-02-20 determined using the methods described in Sections 3.2.5 and 2.2.2. For both the IRF and Esrange lidar the optical

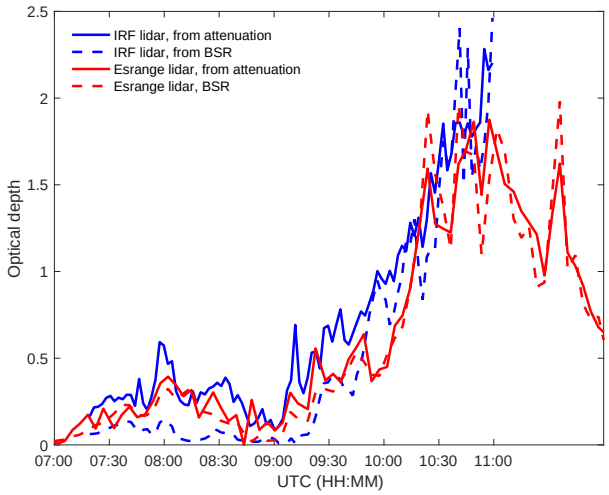

Figure 10. As Fig. 6, but for 2013-02-20.

depths from the two methods seem to agree much better on this day. This indicates that the assumed lidar ratio, as already speculated in Sect. 3.3.2, is indeed better on 2013-02-20 than on 2016-02-12. For the Esrange lidar the agreement seems very good, so that $L_{\mathrm{cirrus}} = 20\,\mathrm{sr}$ is the best lidar ratio resulting from this optical depth comparison. For the IRF lidar, $L_{\mathrm{cirrus}} = 20\,\mathrm{sr}$ also seemed a good assumption for the whole measurement period on 2013-02-20. However, in the earlier hours (7:00 to 9:30 UTC) a somewhat higher lidar ratio would have yielded a better agreement.

4. CONCLUSIONS AND FURTHER WORK

We have shown the first collocations of our ongoing balloon-borne cirrus campaign that started in 2012. A comparison between in-situ measurements and ground-based lidar measurements has been presented for two days of the campaign. In general, good agreement in extinction coefficients and optical depths from in-situ and remote sensing was observed when a suitable lidar ratio was selected. While this best lidar ratio was approximately 20 sr on a day with small particles (2013-02-20), it was larger, around 40 sr, on the other day (2016-02-12), on which larger particles were observed by the in-situ measurements. This agrees with a dependence of lidar ratio on ice particle size observed by [23].

This shows how combining our in-situ measurements with concurrent ground-based lidar measurements provide data that complement each other. While the in-situ measurements provide detailed information of the microphysical properties of the cirrus probed by balloon, the lidar serves also to characterize the temporal and spatial evolution of the cirrus that we sampled.

The comparison of extinction coefficients and optical depth, quantities derived from both in-situ data and lidar measurements is somewhat difficult because exact collocations in time and space cannot easily be achieved. The smallest collocation distances in our measurements are on the order of 20 min and 20 km. While this may be satisfactory under certain conditions, it may be too far under different conditions. Thus, a more carful analysis of the meteorological conditions on the measurement days will be necessary to evaluate how homogeneous or not cirrus layers are in spatial dimensions and how they evolve over time.

Therefore, rather than in a direct comparison of extinction coefficients, a major benefit of having concurrent lidar observations with our in-situ measurements will be in the further studies that are possible. So far we have not used the information on the polarization of the backscattered light that the lidar can provide. Depending on the shape of ice particles, the scattered light measured by lidar is more or less polarized. Thus, we will compare also the lidar depolarization ratios with the observed shapes, which could aid a determination of dominant shapes from lidar depolarization ratios. The lidar ratio will also be studied more in detail by looking at relationships between lidar ratio and cloud microphysical properties from in-situ measurements. In addition to looking at effects of particle size on the lidar ratio, we can also look at the effects of the shape on it. If the lidar ratio can be determined more directly and accurately, then this can reduce uncertainties in lidar derived quantities. In addition, one may infer certain microphysical properties such as dominant shape or size from lidar ratios. For this, the lidar ratio could be derived independently from the vibrational Raman channel [19] of the Esrange lidar. This will require night-time measurements with less stray light. Such night-time measurements would also have the additional benefit of much reduced signal-to-noise ratios in all lidar data. All this planned future work will help to provide better ice cloud properties from lidar-only measurements of cirrus at high latitudes.

ACKNOWLEDGMENTS

We thank Swedish National Space Board for funding this balloon campaign, and Andrew Heymsfield and National Center for Atmospheric Research (NCAR, USA) for their support.

REFERENCES

[1] B. A. Baum, P. Yang, A. J. Heymsfield, C. G. Schmitt, Y. Xie, A. Bansemer, Y. X. Hu, and Z. Zhang. Improvements in shortwave bulk scattering and absorption models for the remote sensing of

ice clouds. *J. Appl. Meteorol. Clim.*, 50:1037–1056, 2011.

[2] M. J. McGill, L. Li, W. D. Hart, G. M. Heymsfield, D. L. Hlavka, P. E. Racette, L. Tian, M. A. Vaughan, and D. M. Winker. Combined lidar-radar remote sensing: Initial results from CRYSTAL-FACE. *J. Geophys. Res.*, 109(D7), 2004.

[3] P. Eriksson, M. Ekström, B. Rydberg, and D. Murtagh. First Odin sub-mm retrievals in the tropical upper troposphere: ice cloud properties. *Atmos. Chem. Phys.*, 7:471–483, 2007.

[4] A. Heymsfield, C. Schmitt, and A. Bansemer. Ice cloud particle size distributions and pressure-dependent terminal velocities from in situ observations at temperatures from 0 to -86 C. *J. Atmos. Sci.*, 2013.

[5] A. V. Korolev, E. F. Emery, J. W. Strapp, S. G. Cober, G. A. Isaac, M. Wasey, and D. Marcotte. Small ice particles in tropospheric clouds: fact or artifact? airborne icing instrumentation evaluation experiment. *Bull. Amer. Met. Soc.*, 92(8):967–973, 2011.

[6] Alexei Korolev, Edward Emery, and Kirk Creelman. Modification and tests of particle probe tips to mitigate effects of ice shattering. *Journal of Atmospheric and Oceanic Technology*, 30(4):690–708, 2013.

[7] R. C. Jackson, G. M. McFarquhar, J. Stith, M. Beals, R. A. Shaw, J. Jensen, J. Fugal, and A. Korolev. An assessment of the impact of anti-shattering tips and artifact removal techniques on cloud ice size distributions measured by the 2d cloud probe. *J. Atmos. Oceanic Technol.*, 31:2567–2590, 2014.

[8] Alexei Korolev. Reconstruction of the sizes of spherical particles from their shadow images. Part I: theoretical considerations. *J. Atmos. Oceanic Technol.*, 24(3):376–389, 2007.

[9] M. T. Stoelinga, J. D. Locatelli, and C. P. Woods. The occurrence of "Irregular" ice particles in stratiform clouds. *J. Atmos. Sci.*, 64(7):2740–2750, 2007.

[10] L. M. Miloshevich and A. J. Heymsfield. A balloon-borne continuous cloud particle replicator for measuring vertical profiles of cloud microphysical properties: Instrument design, performance, and collection efficiency analysis. *J. Atmos. Oceanic Technol.*, 14(4):753–768, 1997.

[11] Thomas Kuhn and Andrew J. Heymsfield. In situ balloon-borne ice particle imaging in high-latitude cirrus. *Pure Appl. Geophys.*, 173(9):3065–3084, 2016.

[12] C. Schiller, M. Kraemer, A. Afchine, N. Spelten, and N. Sitnikov. Ice water content of Arctic, mid-latitude, and tropical cirrus. *J. Geophys. Res.*, 113, DEC 24 2008.

[13] J.-F. Gayet, I. S. Stachlewska, O. Jourdan, V. Shcherbakov, A. Schwarzenboeck, and R. Neuber. Microphysical and optical properties of precipitating drizzle and ice particles obtained from alternated lidar and in situ measurements. *Annales Geophysicae*, 25(7):1487–1497, 2007.

[14] T. Kuhn, A. J. Heymsfield, and S. A. Buehler. Balloon-borne measurements of ice particle shape and ice water content in the upper troposphere over northern Sweden. *Proc. 21st ESA Symposium on European Rocket and Balloon Programmes and Related Research*, SP-721:93–97, 2013.

[15] P. Voelger and G. Nikulin. The new lidar system at the swedish institute of space physics in kiruna: description and first measurements. *17th ESA Symposium on European Rocket and Balloon Programmes and Related Research*, ESA SP-590:321–325, 2005.

[16] U. Blum and K. H. Fricke. The Bonn University lidar at the Esrange: technical description and capabilities for atmospheric research. *Ann. Geophys.*, 23(5):1645–1658, 2005.

[17] T. Kanitz, A. Ansmann, R. Engelmann, and D. Althausen. North-south cross sections of the vertical aerosol distribution over the atlantic ocean from multiwavelength raman/polarization lidar during polarstern cruises. *J. Geophys. Res. Atmos.*, 118(6):2643–2655, 2013.

[18] J. D. Klett. Stable analytical inversion solution for processing lidar returns. *Appl. Opt.*, 20:211–220, 1981.

[19] A. Ansmann, U. Wandinger, M. Riebesell, C. Weitkamp, and W. Michaelis. Independent measurement of extinction and backscatter profiles in cirrus clouds by using a combined raman elastic-backscatter lidar. *AO*, 31(33):7113–7131, 1992. Cited By :432.

[20] J. Reichardt, S. Reichardt, M. Hess, and T. J. McGee. Correlations among the optical properties of cirrus-cloud particles: Microphysical interpretation. *JGR*, 107(21):XL, 2002. Cited By :16.

[21] R. Kuehn, R. Holz, E. Eloranta, M. Vaughan, and J. Hair. Developing a climatology of cirrus lidar ratios using University of Wisconsin HSRL observations. In *EPJ Web of Conferences*, volume 119, 2016.

[22] M. Saito, H. Iwabuchi, P. Yang, G. Tang, M. D. King, and M. Sekiguchi. Ice particle morphology and microphysical properties of cirrus clouds inferred from combined caliop-iir measurements. *JGR*, 122(8):4440–4462, 2017.

[23] J. F Gayet, G. Febvre, G. Brogniez, H. Chepfer, W. Renger, and P. Wendling. Microphysical and optical properties of cirrus and contrails: Cloud field study on 13 october 1989. *JAS*, 53(1):126–138, 1996. Cited By :78.